PHYSICS OF FLUIDS **26**, 054104 (2014)

Mechanisms of mean flow formation and suppression in two-dimensional Rayleigh-Bénard convection

Joseph G. Fitzgerald[a] and Brian F. Farrell
Department of Earth and Planetary Sciences, Harvard University, Cambridge, Massachusetts 02138, USA

(Received 16 October 2013; accepted 29 April 2014; published online 27 May 2014)

Two-dimensional laminar roll convection is capable of generating energetic horizontal mean flows via a well-understood process known as the tilting instability. Less well-understood is the physical mechanism behind the strong dependence of this effect on the horizontal lengthscale of the convection pattern. Mean flows of this type have been found to form for sufficiently large Rayleigh number in periodic domains with a small aspect ratio of horizontal length to vertical height, but not in large aspect ratio domains. We demonstrate that the elimination of the tilting instability for large aspect ratio is due to a systematic eddy-eddy advection mechanism intervening at linear order in the tilting instability, and that this effect can be captured in a model retaining two nonlinearly interacting horizontal wavenumber components of the convection field. Several commonly used low-order models of convection also exhibit a shutdown of the tilting instability for large aspect ratio, even though these models do not contain the eddy-eddy advection mechanism. Instability suppression in such models is due to a different mechanism involving vertical advection. We show that this vertical advection mechanism is excessively strong in the low-order models due to their low resolution, and that the instability shutdown in such models vanishes when they are appropriately extended. © *2014 AIP Publishing LLC*. [http://dx.doi.org/10.1063/1.4875814]

I. INTRODUCTION

It is well known that two-dimensional (2D) convection can give rise to spontaneous formation of strong horizontal mean flows. In Rayleigh-Bénard convection, this phenomenon is controlled by three nondimensional external parameters: the Rayleigh number Ra which measures the strength of the thermal driving, the Prandtl number Pr which is the nondimensional ratio of kinematic viscosity to thermal diffusivity, and the domain aspect ratio Γ which specifies the problem geometry. As Ra is increased, the system transitions from an unstably stratified conductive state to a state in which heat is transported by laminar convection rolls. As Ra is further increased in a horizontally periodic domain, this roll state may undergo a symmetry-breaking transition to a state with a horizontal mean flow co-existing with tilted convection rolls. Subsequent transitions can result in oscillating mean flows and chaotic behavior.

Convection-driven mean flow formation has been identified in a wide variety of physical models. Thompson[1] originally obtained energetic mean shear flows in a 2D model of convection in the Venusian atmosphere. Subsequent studies of the Rayleigh-Bénard system with both free-slip[2,40] and no-slip[3,37] boundary conditions, convection driven by internal heating,[4] compressible convection,[5,6] and magnetoconvection[7–9] demonstrated that mean flow formation occurs quite generally in 2D systems that produce roll convection. The dynamics of 2D convection is also closely related to that of the resistive interchange modes of magnetically confined plasmas,[10] and mean flow formation in convective systems is often associated with the transition between the low- and high-confinement states in tokamaks.[11]

[a]Electronic mail: jfitzgerald@fas.harvard.edu

Convection in 2D has most often been studied numerically, as 2D systems are difficult to access with experiments. The transition to tilted cells with a mean flow has been observed, however, in experimental studies of Hele-Shaw convection[12] and electromagnetically driven vortices,[13] two systems in which the dynamics are close to 2D. The theoretical and experimental examples listed above indicate that mean flow formation is a robust phenomenon in these 2D or nearly 2D convection systems. However, mean flows of this type, which bifurcate from a state of laminar convection, have not been found to form in 3D Rayleigh-Bénard convection. This difference in mean flow formation between 2D and 3D convection exists in spite of the fact that 2D rolls, the state preceding mean flow development in the 2D system, do form in 3D geometries at low *Ra*. The absence of mean flow formation from 2D laminar rolls in the 3D system has been attributed to the preemption of the transition from 2D rolls to the mean flow state by a transition from 2D to 3D convection that occurs first as *Ra* is increased.[14]

The physical mechanism of mean flow formation by 2D convection was first identified by Thompson.[1] In a horizontally periodic domain, a horizontal mean flow must be supported against diffusion by a Reynolds stress. In the convection system, this Reynolds stress is provided by tilted convection rolls. The transition from untilted ("symmetric") convection to tilted convection proceeds as follows. To an initially symmetric convection state an infinitesimal mean shear flow perturbation is added. This perturbation advects the rolls, causing them to become tilted with the shear. The tilted rolls now have an associated Reynolds stress which transports momentum upgradient, reinforcing the initial shear flow. Through this feedback process, shear perturbations may grow in amplitude upon a background state of laminar convection. This "tilting mechanism" differs from an inverse cascade of energy to large scales.[15] In the tilting instability, energy is transferred directly from the convective scale to the mean flow without a nonlinearly mediated cascade.

Although the tilting mechanism has been verified to operate in numerical simulations[2] and theoretical models,[12] some questions remain. It has always been found that mean flows form readily in periodic domains with small aspect ratio of horizontal length to vertical height $\Gamma = L/H$.[9] For larger Γ, mean flows of this type do not form, with their development being replaced by strengthening of the convective circulation and thinning of boundary layers as Ra is increased until the eventual breakdown of the rolls into turbulent plume convection.[16] The value of Γ determines the set of nondimensional horizontal wavenumbers $\hat{k}_n = Hk_n = 2\pi n/\Gamma$ allowed by the periodic geometry. Convection driven by an imposed temperature gradient sets in at low *Ra* in the form of rolls taking on the allowable $\hat{k}$ that has the lowest critical value of *Ra*. For small Γ, this constrains the rolls to be of large $\hat{k}$, while for larger Γ, convection sets in at a lower value of $\hat{k}$ near the minimum of $Ra_{crit}(\hat{k})$.[17] The absence of mean flows for large Γ is then consistent with the theoretical predictions of Busse,[18] who showed that mean flows are only generated for sufficiently strong rolls of sufficiently large $\hat{k}$ (which corresponds to sufficiently small Γ). This strong scale dependence does not follow in an obvious way from the tilting mechanism described above.

Low-order models (LOMs), in which the equations of motion are projected onto a truncated Galerkin expansion in the spirit of Lorenz,[19] have been a popular theoretical tool for the study of mean flow generation. Motivated by laboratory experiments in a three-dimensional annulus,[20] Howard and Krishnamurti[12] (hereafter HK86) first took such an approach, augmenting the Lorenz system with three additional Fourier components corresponding to the mean flow and the tilting of the buoyancy and vorticity fields. The tilting instability occurs for all Γ in the HK86 model. Hermiz *et al.*[21] (hereafter H95) extended HK86, adding an additional component to enforce vorticity conservation, and found that the tilting instability was "cut off" for large-Γ, low-*Pr* so that mean flows were no longer formed for any *Ra*. Thiffeault and Horton[22] and Gluhovsky *et al.*[23,24] also studied extensions of HK86, adding components to conserve energy and to produce a model with the properties of a Volterra gyrostat. Similar LOMs have been applied to vortex instability in the absence of a buoyancy field. Finn *et al.*[11] and Drake *et al.*[25] analyzed a four-component model of the buoyancy-free tilting instability which included a vorticity-conserving component and found that the mean flow instability was cut off for large Γ, consistent with the results of H95. Mean flow formation by magnetoconvection has also been studied using LOMs,[26] with particular attention being paid to the small-Γ limit.[27]

LOMs have typically represented the dynamics in a reduced basis consisting of a single horizontal wavenumber component $\hat{k}$ and vertical components chosen to allow tilted convection and to enforce desired conservation properties. This approach is a natural one since the laminar roll state preceding mean flow development is often well-characterized by a single horizontal Fourier component. Additionally, Rosenbluth and Shapiro[28] showed that higher horizontal components were formally suppressed in the low-Γ limit of a nonlinear model of unforced vortices, and Soloviev and Shapiro[29] generalized their analysis to include the effects of buoyancy. These theoretical results provide a justification for single-$\hat{k}$ truncations when applied to low-Γ domains. Beyond the low-Γ limit, however, the influence of higher wavenumber components has yet to be clarified.

Two-dimensional Rayleigh-Bénard convection has served as the canonical conceptual example of mean flow formation by convection for more than 40 years, and the study of this system has contributed understanding to a wide range of fields including meteorology, laboratory fluid dynamics, astrophysical convection, and plasma physics. Despite this progress, important aspects of the mean flow formation process remain poorly understood, even in this idealized example. The primary motivation of this work is to demonstrate the physical mechanism responsible for the observed, but previously unexplained, shutdown of the tilting instability for sufficiently large aspect ratio. We identify this mechanism with a systematic eddy-eddy-advection process which intervenes at linear order in the tilting instability. A secondary motivation of this work is to clarify the relationship between the physical mechanisms operating in LOMs, which can also exhibit shutdown of tilting as Γ increases, and those operating in the full nonlinear dynamics. We show that a class of simple models predicting a shutdown of the tilting instability at large Γ do so due to a different mechanism than that operating in the full system. Furthermore, we show that this alternate mechanism, a vertical advection feedback between the mean flow and the convection, is excessively strong in such simple models and weakens when they are made more realistic, removing the instability shutdown in these models.

The paper is organized as follows. In Sec. II, we present the nonlinear equations of motion for Rayleigh-Bénard convection and formulate quasilinear (mean-field) and low-order approximations to the dynamics. In Sec. III, we present results from the nonlinear system demonstrating the suppression of mean flow formation for large Γ and explain the physical mechanism of this phenomenon. In Sec. IV, we formulate a model of two nonlinearly interacting Fourier components of convection and demonstrate that this model captures important features of the instability suppression occurring in the full nonlinear system. In Sec. V, we address mean flow suppression in LOMs. We first illustrate the mechanism that eliminates the mean flow instability for large Γ in LOMs using H95 together with the quasilinear model. We further show that an instability cutoff does not occur in the quasilinear model, and that the cutoff present in LOMs can be removed by increasing model resolution. We summarize and discuss our results in Sec. VI.

II. MODEL FORMULATION

A. Nonlinear dynamics

The nondimensional nonlinear equations of motion for a 2D incompressible Boussinesq fluid confined between two perfectly conducting free-slip horizontal plates at $z = 0$ and $z = H$ are

$$\frac{1}{Pr}\left(\frac{\partial}{\partial t} + \mathbf{u}\cdot\boldsymbol{\nabla}\right)\boldsymbol{\nabla}^2\psi = Ra\frac{\partial\theta}{\partial x} + \boldsymbol{\nabla}^4\psi, \tag{1}$$

$$\left(\frac{\partial}{\partial t} + \mathbf{u}\cdot\boldsymbol{\nabla}\right)\theta = w + \boldsymbol{\nabla}^2\theta. \tag{2}$$

We refer to these nonlinear equations of motion using the abbreviation "NL". Here, ψ is the streamfunction such that $\mathbf{u} = (u, w) = (-\psi_z, \psi_x)$ are the horizontal and vertical components of velocity, θ is the deviation of the buoyancy from a background linear conductive profile, and $\boldsymbol{\nabla}^2 = \partial_{xx} + \partial_{zz}$. The Rayleigh number and Prandtl number are defined as

$$Ra = \frac{\alpha g \Delta T H^3}{\nu\kappa}, \qquad Pr = \frac{\nu}{\kappa}, \tag{3}$$

where H is the domain height, α is the coefficient of thermal expansion, g is the acceleration due to gravity, ΔT is the imposed temperature difference between the bottom and top plates, ν is the kinematic viscosity, and κ is the thermal diffusivity. Space has been nondimensionalized by the domain height $\mathbf{x} = H\hat{\mathbf{x}}$, time by the thermal diffusion timescale $t = (H^2/\kappa)\hat{t}$, velocity by $\mathbf{u} = (\kappa/H)\hat{\mathbf{u}}$, and buoyancy by the imposed gradient $\theta = (\alpha g \Delta T)\hat{\theta}$. Carets have been dropped. The boundary conditions are $\theta = w = u_z = 0$ at $z = 0$, 1 and periodic in the x direction with nondimensional periodicity length $\Gamma = L/H$, the domain aspect ratio. We typically measure the thermal forcing strength using the relative Rayleigh number $r = Ra/Ra_{crit}$, where $Ra_{crit} = \min[(k^2 + \pi^2)^3/k^2]$ is the value of Ra at which the conduction state becomes unstable to roll convection, with the minimization performed over all horizontal wavenumbers $k_n = 2\pi n/\Gamma$ permitted by the periodic geometry. We show results from the parameter range $0.5 \leq \Gamma \leq 4$ for which the gravest horizontal component $k_1 = 2\pi/\Gamma$ is the first to go unstable as Ra is increased.

To study mean flow formation, we perform a Reynolds decomposition to write separate equations of motion for horizontal mean quantities (denoted by overbars) and deviations from the horizontal mean (denoted by primes). The resulting equations of motion are

$$\frac{\partial \overline{u}}{\partial t} = -\frac{\partial}{\partial z}\overline{u'w'} + Pr\frac{\partial^2 \overline{u}}{\partial z^2}, \tag{4}$$

$$\frac{\partial \overline{\theta}}{\partial t} = -\frac{\partial}{\partial z}\overline{w'\theta'} + \frac{\partial^2 \overline{\theta}}{\partial z^2}, \tag{5}$$

$$\frac{\partial}{\partial t}\nabla^2\psi' = -\overline{u}\frac{\partial}{\partial x}\nabla^2\psi' + w'\frac{\partial^2 \overline{u}}{\partial z^2} + Ra\,Pr\frac{\partial \theta'}{\partial x} + Pr\nabla^4\psi' + (\mathrm{EENL})_\psi, \tag{6}$$

$$\frac{\partial \theta'}{\partial t} = -\overline{u}\frac{\partial \theta'}{\partial x} - w'\frac{\partial \overline{\theta}}{\partial z} + w' + \nabla^2\theta' + (\mathrm{EENL})_\theta. \tag{7}$$

Here, we refer to the individual contributions to the partial time derivatives of eddy vorticity and buoyancy, i.e., terms appearing on the right hand sides of (6) and (7), as vorticity and buoyancy tendencies. In particular, the EENL terms in (6) and (7) refer to the eddy-eddy nonlinear vorticity and buoyancy tendencies[30]

$$(\mathrm{EENL})_\psi \equiv -J(\psi, \nabla^2\psi)', \tag{8}$$

$$(\mathrm{EENL})_\theta \equiv -J(\psi, \theta)'. \tag{9}$$

Here, we have used the notation $J(f, g) = (\partial_x f)(\partial_z g) - (\partial_z f)(\partial_x g)$ for the Jacobian operator and $J(f, g)' = J(f', g') - \overline{J(f', g')}$ for the EENL component of the Jacobian. We refer to the primed quantities in (4)–(7) as the convection and to the horizontal mean quantities as the mean flow and mean buoyancy profile. These equations of motion were solved numerically using a Fourier Galerkin expansion in x and a finite difference discretization in z. For such a method resolution is determined by the number of retained horizontal Fourier components M as well as the number of gridpoints in the z direction N. The resolution was set at $(M, N) = (16, 32)$, which was found to be sufficient for the cases considered here.

B. Quasilinear dynamics

The tilting instability described in Sec. I results from the interactions between the convection rolls and the mean flow. This suggests a theoretical model in which these interactions are retained but the remaining nonlinearities are discarded, usually referred to as the quasilinear[4] or mean-field[31] approach. The quasilinear dynamics is obtained by neglecting the EENL terms in (6) and (7). The prognostic equations for primed variables then become linear in primed quantities so that higher horizontal wavenumber components are not nonlinearly generated by lower wavenumbers through the EENL terms. Retaining a single horizontal wavenumber component in the Fourier expansion of

the convection fields,

$$\psi = \mathrm{Re}\left[\tilde{\psi}_k(z,t)e^{ikx}\right], \qquad \theta = \mathrm{Re}\left[\tilde{\theta}_k(z,t)e^{ikx}\right], \tag{10}$$

with $k = 2\pi n/\Gamma$ for a positive integer n, the QL equations of motion become

$$\frac{\partial \overline{u}}{\partial t} = -k\frac{1}{2}\frac{\partial}{\partial z}\mathrm{Im}\left[\tilde{\psi}_k\frac{\partial \tilde{\psi}_k^*}{\partial z}\right] + Pr\frac{\partial^2 \overline{u}}{\partial z^2}, \tag{11}$$

$$\frac{\partial \overline{\theta}}{\partial t} = k\frac{1}{2}\frac{\partial}{\partial z}\mathrm{Im}\left[\tilde{\psi}_k\tilde{\theta}_k^*\right] + \frac{\partial^2 \overline{\theta}}{\partial z^2}, \tag{12}$$

$$\frac{\partial}{\partial t}\nabla^2\tilde{\psi}_k = -ik\overline{u}\nabla^2\tilde{\psi}_k + ik\tilde{\psi}_k\frac{\partial^2 \overline{u}}{\partial z^2} + ikRaPr\tilde{\theta}_k + Pr\nabla^4\tilde{\psi}_k, \tag{13}$$

$$\frac{\partial \tilde{\theta}_k}{\partial t} = -ik\overline{u}\tilde{\theta}_k - ik\tilde{\psi}_k\frac{\partial \overline{\theta}}{\partial z} + ik\tilde{\psi}_k + \nabla^2\tilde{\theta}_k, \tag{14}$$

in which * denotes complex conjugation, $\nabla^2 = (-k^2 + \partial_{zz})$, and Re and Im indicate the real and imaginary parts, respectively. We refer to these quasilinear equations of motion using the abbreviation "QL".

The QL equations for convection were previously used by Herring,[31] who explicitly excluded the possibility of mean flow formation, to study the finite-amplitude equilibration of convection rolls. More recently, the single-k QL model was applied by Bian *et al.*[4] to study 2D source-driven convection in plasmas. Additional wavenumber components could in principle be included in the QL dynamics. However, Soloviev and Shapiro[29] showed that, for low-Γ convection, a single k contributes to the dynamics while all higher wavenumbers are suppressed. For larger Γ, we will show that the most significant effects of additional wavenumbers with respect to mean flow formation result from the EENL terms, rendering the QL equations a poor model for the system in this parameter regime. Accordingly, we will use the QL model in the single-k formulation only. We retain the $n = 1$ component, so that convection occurs on the largest scale permitted by the periodic boundary conditions. The first component of convection is typically the dominant one in the NL dynamics in the low-Ra, moderate-Γ parameter regime considered here, making $n = 1$ an appropriate choice for the QL approximation.

C. Low-order dynamics

The QL model retains a single horizontal component k but places no restrictions on vertical structure. A common approach has been to instead expand the streamfunction and buoyancy in a truncated Fourier series in both x and z to obtain a LOM consisting of several ordinary differential equations for the expansion coefficients. The most general formulation of such a model expands ψ and θ as

$$\psi(x,z,t) = \sum_{n=0}^{\infty}\sum_{m=1}^{\infty}\left(A_{nm}(t)\cos(k_n x) + B_{nm}(t)\sin(k_n x)\right)\sin(m\pi z), \tag{15}$$

$$\theta(x,z,t) = \sum_{n=0}^{\infty}\sum_{m=1}^{\infty}\left(C_{nm}(t)\cos(k_n x) + D_{nm}(t)\sin(k_n x)\right)\sin(m\pi z), \tag{16}$$

in which the A_{0m} coefficients encode the mean flow structure. Use of the sine series in the vertical is due to our free-slip and perfectly conducting boundary conditions at the top and bottom, which also restricts the total linear momentum of the system to be zero if it is initialized as such. Mean flow formation can occur with both free-slip and no-slip boundary conditions, and mean flow behavior in the no-slip case was studied by Prat *et al.*[3,37] Typically, LOMs retain the single horizontal component $n = 1$ alongside the mean flow and buoyancy profile $n = 0$ and a selection of vertical components m chosen based on physical reasoning. The most well-known LOM is the HK86 model which retains

the components ($A_{01,12}$, B_{11}, $C_{02,11}$, D_{12}) and produces a mean flow for all values of Γ. Several extensions of HK86, however, exhibit a shutdown of the tilting instability when Γ is sufficiently increased. In particular, the H95 LOM augments HK86 to include the A_{03} component and exhibits a cutoff of the tilting instability for sufficiently large Γ and low *Pr*. We will examine the mechanism of mean flow suppression in LOMs in Sec. V.

III. MECHANISM OF ELIMINATION OF THE MEAN FLOW INSTABILITY IN THE NL SYSTEM

In this section, we compare the mean flow formation behavior in the NL and QL systems in both low- and high-Γ parameter regimes. Using the observed differences in behavior as a guide, we identify the physical mechanism responsible for the elimination of the mean flow instability in the NL system for all *r* given sufficiently large Γ with a negative feedback arising from EENL interactions which are excluded from the QL model. Figures 1(a)–1(c) show the results of both NL and QL integrations for low-Γ, marginally supercritical convection with (Γ, *Pr*, *r*) = (0.5, 1, 1.1). Panel (a) shows the time series of domain-averaged kinetic energies of the convection $\frac{1}{2}\langle u'^2 + w'^2\rangle$ and of the mean flow $\frac{1}{2}\langle \overline{u}^2\rangle$. Following initialization at $t = 0$ by a small-amplitude perturbation, the convection first grows rapidly as part of the usual Rayleigh-Bénard instability. Subsequently, convection saturates due to the erosion of the background buoyancy gradient by convective heat transport. Upon this background of symmetric (untilted) convection, an initially small mean flow perturbation grows exponentially via the tilting mechanism and subsequently equilibrates to produce a final state of tilted convection alongside a finite-amplitude mean flow (Figs. 1(b) and 1(c)). Circles in (a) and (c) show the behavior of the NL model, which agrees quantitatively with QL for these

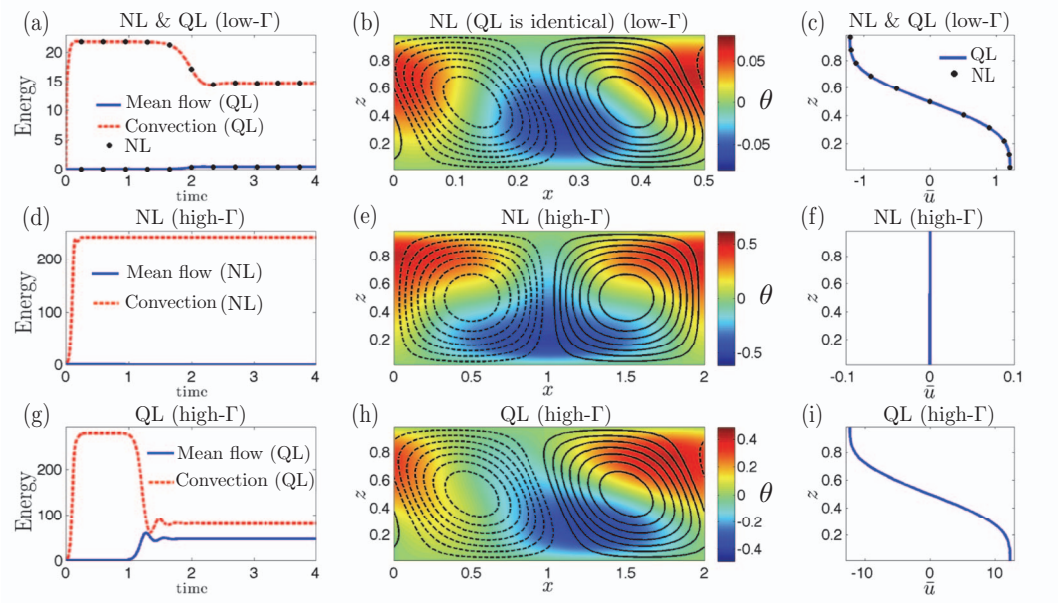

FIG. 1. Comparison of mean flow formation behavior in the NL and QL systems for low and high aspect ratio (Γ). The top row overlays NL and QL results for the low-Γ case while the lower two rows show separately the NL (middle row) and QL (bottom row) results for the higher-Γ case. Left column: Time series of the convection and mean flow energies for (a) (Γ, *Pr*, *r*) = (0.5, 1, 1.1) and (d) and (g) (Γ, *Pr*, *r*) = (2.0, 1, 5). Center column: Eddy streamlines and full buoyancy fields for the equilibrium state sampled at $t = 4$ for (b) (Γ, *Pr*, *r*) = (0.5, 1, 1.1) and (e) and (h) (Γ, *Pr*, *r*) = (2.0, 1, 5). Solid contours indicate eddy streamlines with counter-clockwise circulation, shading shows the buoyancy field. NL and QL fields are indistinguishable in (b). Right column: Mean flow profile for the equilibrium state sampled at $t = 4$ for (c) (Γ, *Pr*, *r*) = (0.5, 1, 1.1) and (f) and (i) (Γ, *Pr*, *r*) = (2.0, 1, 5). This figure demonstrates that for low Γ (top row) the NL and QL systems agree closely, but that this agreement is lost for higher Γ (middle and bottom rows) for which mean flows no longer form in NL but continue to form in QL.

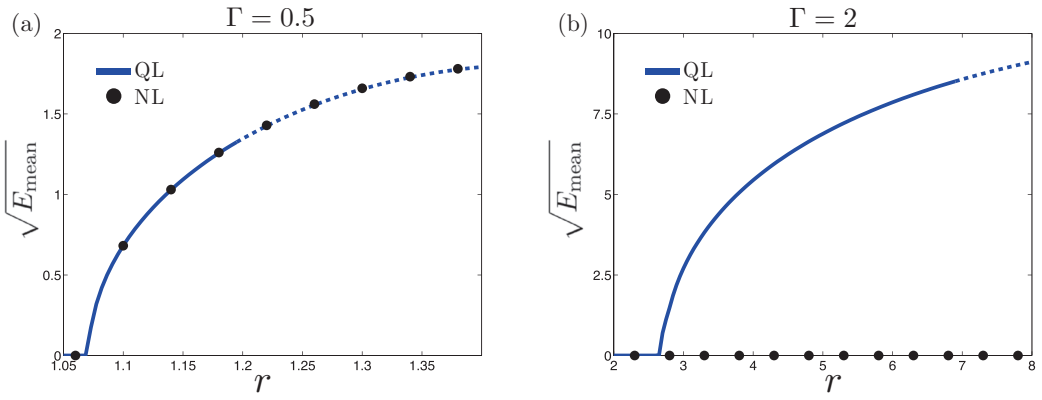

FIG. 2. Mean flow bifurcation diagrams for NL and QL for the two values of Γ shown in Fig. 1 ($Pr = 1$). Solid curves indicate stable equilibria and dashed curves unstable equilibria. For $\Gamma = 0.5$ (a), a mean flow forms in both QL and NL as r is increased beyond $r \approx 1.05$. The mean flow equilibrium becomes unstable near $r \approx 1.2$, giving way to an oscillating mean flow solution in both QL and NL. For $\Gamma = 2$ (b), a mean flow forms in QL beyond $r \approx 2.7$ and begins to oscillate beyond $r \approx 6.9$, while a mean flow does not form in NL. This figure demonstrates that for low Γ the mean flow bifurcation has essentially identical properties in QL and NL, and that for larger Γ the tilting instability is eliminated entirely in NL but continues to occur in QL.

parameter values. Figure 2(a) shows the mean flow bifurcation diagram for $\Gamma = 0.5$ obtained by numerical continuation. Mean flows form as r is increased beyond $r \approx 1.05$ in both QL and NL, which have essentially identical mean flow properties over a range of r for this aspect ratio.

The agreement between the NL and QL dynamics for $\Gamma = 0.5$ is not maintained for larger Γ. Panels (d)-(f) of Fig. 1 show the behavior of the NL system for $(\Gamma, Pr, r) = (2.0, 1, 5)$, while (g)-(i) show the behavior of the QL system for the same parameter values. In this case, a strong mean flow forms in QL, while no such mean flow forms in NL. Figure 2(b) shows the mean flow bifurcation diagram for $\Gamma = 2$ in NL and QL, and demonstrates that for this higher Γ, the mean flow instability is eliminated altogether in NL so that a mean flow is not formed for any r. On the other hand, the instability is not eliminated in QL, with the increase in Γ instead displacing the mean flow bifurcation point from $r \approx 1.05$ for $\Gamma = 0.5$ to $r \approx 2.7$ for $\Gamma = 2$.

Given the strong driving mechanism for mean flow formation in this system it is natural to ask what mechanism stabilizes convection against mean flow formation in NL. Several candidates are available. Diffusion processes directly damp both the mean flow and the convective perturbations associated with tilting. As we will discuss in more detail in Sec. V, vertical advection of the mean vorticity profile by the background roll circulation also suppresses tilting. However, the QL system contains these mechanisms but continues to form mean flows for large Γ for sufficiently large r while NL does not. This indicates that, although diffusion and vertical advection do contribute to mean flow suppression in NL, the mechanism resulting in instability elimination in NL is connected to the EENL terms that have been neglected in the QL system.

To identify the particular stabilizing feedback responsible for instability elimination in the NL system, we perform a forcing experiment in which a body force is temporarily applied to drive a mean flow for $(\Gamma, Pr, r) = (2.0, 1, 5)$. For these parameter values, symmetric convection is stable in the absence of the body force, and the convective equilibrium state is shown in Fig. 1(e). Figure 3 shows the time evolution during the forcing experiment of the mean flow and the $n = 1$ and $n = 2$ horizontal Fourier components of convection. Initially, the convective energy grows before equilibrating at finite amplitude. In this equilibrium, the $n = 2$ energy is maintained by EENL interactions involving the $n = 1$ component. During the interval $t \in [1, 1.5]$ (shaded) the mean flow is subjected to a body force $F(z) = 5\cos(\pi z)$ (i.e., this $F(z)$ is added to the right hand side of (4)). In addition to the expected increase in mean flow energy during this interval, the $n = 2$ energy also increases relative to its equilibrium level. When the body force is removed at $t = 1.5$ the mean flow decays exponentially to zero and the $n = 2$ component returns to its previous equilibrium strength. This connection between the variation of the mean flow and that of the $n = 2$ component

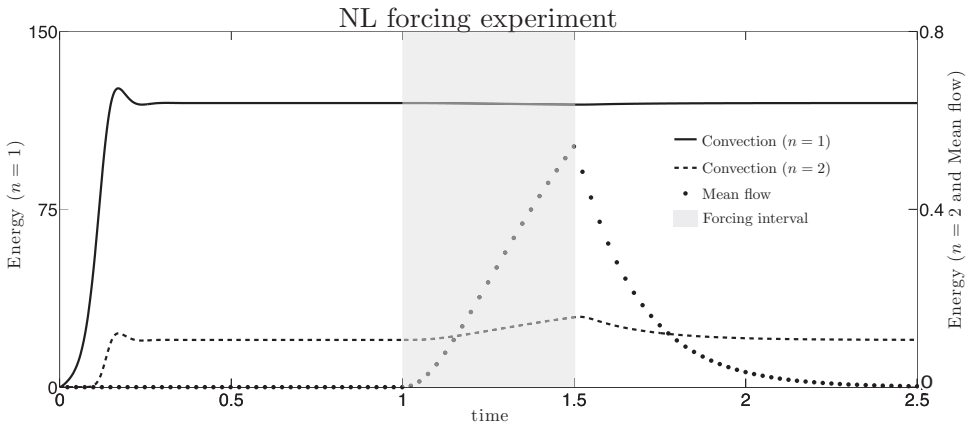

FIG. 3. Evolution of the energies of the mean flow and the $n = 1$ and $n = 2$ convection components during a forcing experiment with NL in which the mean flow is driven with a body force over the interval $t \in [1, 1.5]$ (shaded). The experiment is conducted for $(\Gamma, Pr, r) = (2.0, 1, 5)$, parameter values for which the symmetric convection state is stable to mean flow perturbations (cf. Fig. 1(e)). This figure demonstrates that the $n = 2$ component grows together with the mean flow during the forced phase and decays together with the mean flow during the decay phase, suggesting that the $n = 2$ component is involved in the dynamics of mean flow suppression in the NL system.

suggests that the $n = 2$ component is involved in the mean flow suppression mechanism in NL. We wish to note that the forcing we apply acts to produce a mean flow that is antisymmetric in the vertical about $z = 1/2$. This forcing is consistent with the antisymmetry of the mean flows arising from the tilting instability at low to moderate r seen in Figs. 1(c) and 1(h).[32]

To clarify the role played by the $n = 2$ component of convection in the suppression of mean flow formation in NL, we show in Fig. 4 a collection of structures and tendencies (contributions to the partial time derivative of vorticity) sampled from the forcing experiment at $t = 1.8$ during the

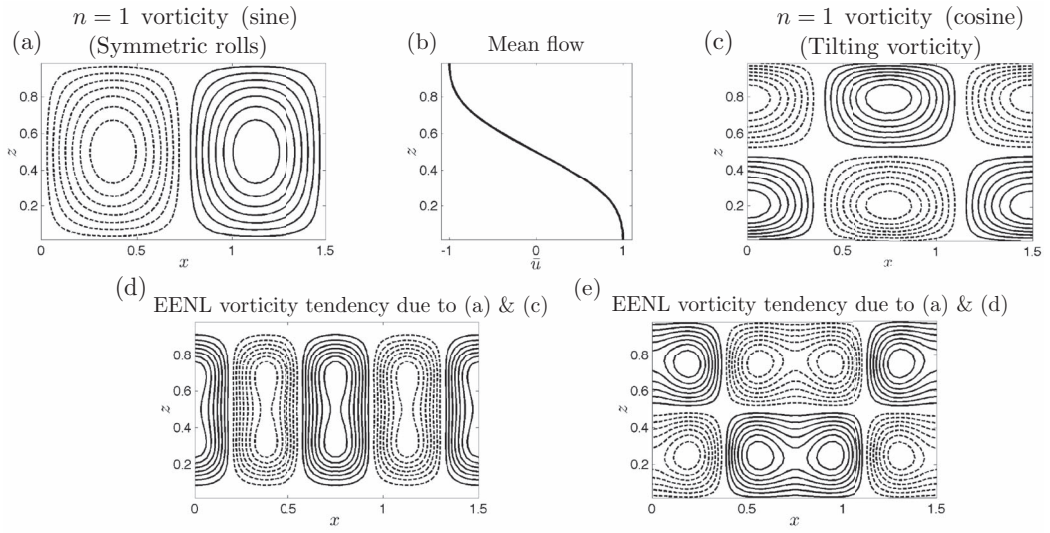

FIG. 4. Structures and tendencies involved in the mean flow suppression mechanism in the NL system. Samples were taken from the NL forcing experiment at $t = 1.8$ during mean flow decay and normalized to unit amplitude (see Fig. 3). Solid contours indicate positive values. Structures: (a) Symmetric roll vorticity field, (b) mean flow, (c) tilting vorticity field. Tendencies: (d) Vorticity tendency due to the EENL interaction of the symmetric roll with the tilting vorticity. This tendency produces the $n = 2$ vorticity component. (e) Vorticity tendency due to the EENL interaction of the symmetric roll with the $n = 2$ structure resulting from the tendency shown in (d). This tendency is close to the negative of the tilting vorticity field shown in (c), and so suppresses tilting of the rolls. This figure demonstrates the mechanism of negative feedback responsible for the suppression of mean flow formation for all r for sufficiently large Γ in the NL system.

exponential decay of the mean flow. By examining these structures and tendencies, we will identify a mechanism of negative feedback involving the EENL coupling of the $n = 1$ and $n = 2$ components of convection that acts to inhibit mean flow formation. As amplitudes vary with time and are not critical to the description of the mechanism, all patterns in Fig. 4 have been normalized to unit amplitude. For the forcing experiment, the NL system was initialized with a $\sin(\pi z)\sin(k_1 x)$ structure in the vorticity field for visual clarity. With this initialization, the symmetric rolls align with the $n = 1$ sine horizontal Fourier component, while the circulation associated with tilted convection appears as the $n = 1$ cosine component

$$\text{Symmetric rolls: } \psi_1'^s(x, z, t) = -\text{Im}\left[\tilde{\psi}_1(z, t)\right]\sin(k_1 x), \tag{17}$$

$$\text{Tilting component: } \psi_1'^c(x, z, t) = \text{Re}\left[\tilde{\psi}_1(z, t)\right]\cos(k_1 x). \tag{18}$$

Subscripts in (17) and (18) indicate the $n = 1$ horizontal Fourier component, while the superscripts s and c indicate the sine and cosine components. Figures 4(a)-4(c) show the symmetric roll vorticity, the mean flow, and the vorticity field associated with the tilting of convection (hereafter tilting vorticity). These structures are each part of the tilting mechanism and closely resemble the components (B_{11}, $A_{01,\,12}$) included in LOMs.

We now highlight two particular EENL tendencies which together produce an important mean flow suppression feedback in NL. Figure 4(d) shows the first of these tendencies, which results from the EENL interaction of the symmetric rolls $\psi_1'^s$ (Fig. 4(a), Eq. (17)) and the tilting component $\psi_1'^c$ (Fig. 4(c), Eq. (18))

$$(\text{EENL})_{\psi}^{1s,1c} = -J\left(\psi_1^s, \nabla^2\psi_1^c\right)' - J\left(\psi_1^c, \nabla^2\psi_1^s\right)'. \tag{19}$$

This tendency acts to drive a $n = 2$ cosine vorticity field, $\psi_2'^c$. It is this $n = 2$ structure that contains the growing $n = 2$ energy during the forced phase of Fig. 3. Figure 4(e) shows the second tendency, which results from the EENL interaction of the symmetric rolls $\psi_1'^s$ (Fig. 4(a)) and the $n = 2$ vorticity structure $\psi_2'^c$ produced by the tendency shown in Fig. 4(d)

$$(\text{EENL})_{\psi}^{1s,2c} = -J\left(\psi_1^s, \nabla^2\psi_2^c\right)' - J\left(\psi_2^c, \nabla^2\psi_1^s\right)'. \tag{20}$$

It is clear from inspection of Fig. 4(e) that this tendency projects strongly and with negative sign onto the tilting vorticity $\psi_1'^c$ shown in Fig. 4(c). Together, the EENL interactions (19) and (20) produce a negative feedback that suppresses the tilting of convection rolls, weakening the Reynolds stress and inhibiting mean flow formation.

We note that the EENL interaction (19) shown in Fig. 4(d) includes only advective interactions between the (a) and (c) structures and excludes each structure's self-interaction. The self-interaction of the symmetric rolls is responsible for the background level of $n = 2$ energy, while the self-interaction of the tilting vorticity is quadratically small in the perturbation amplitude and plays no role in the mean flow instability process. Likewise, we exclude the self-interaction of each structure from the tendency (20) shown in Fig. 4(e) since they do not play any role in the suppression mechanism to linear order in the perturbation amplitude.

The EENL suppression mechanism results from the interaction of $n = 1$ and $n = 2$ structures. However, the symmetric rolls shown in Fig. 1(e) are well-represented by the $n = 1$ component alone, so that the $n = 2$ structures ultimately responsible for stabilizing symmetric convection are present only weakly in the symmetric roll state itself. For this reason, many previous LOMs retained the $n = 1$ component only, thereby explicitly filtering the EENL suppression mechanism. However, many LOMs exhibit elimination of the mean flow instability at large Γ despite retaining only the $n = 1$ component.[11,21,25] In Sec. V, we will explain the physical mechanism responsible for mean flow suppression in such models, and clarify the relationship between the suppression phenomena in LOMs and NL.

IV. A MODEL OF TWO NONLINEARLY INTERACTING FOURIER COMPONENTS

In Sec. III, we demonstrated the existence of a negative feedback inhibiting mean flow formation involving EENL coupling of the $n = 1$ and $n = 2$ horizontal Fourier components of convection. To

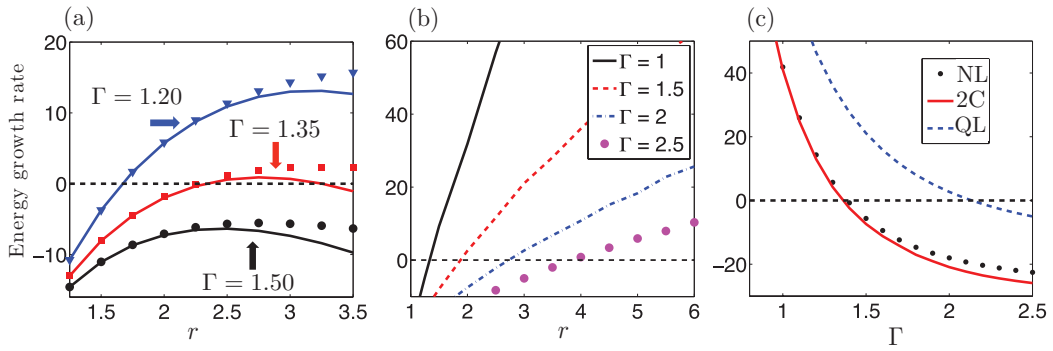

FIG. 5. Comparison of the mean flow energy growth rates in the NL, 2C, and QL systems. (a) NL (discrete symbols) and 2C (continuous curves) growth rates as functions of r for three values of Γ for $Pr = 1$. Important features revealed by this plot are: First, growth rates in 2C agree with those in NL for low r for each Γ. Second, growth rate curves in NL and 2C shift downward as Γ is increased. Third, for $\Gamma = 1.35$ and $\Gamma = 1.50$, growth rates in NL and 2C attain a maximum and subsequently decrease as r is increased. This decreasing behavior results in elimination of the instability for all r for $\Gamma \gtrsim 1.4$. Finally, for $\Gamma = 1.20$ and $\Gamma = 1.35$ growth rate curves in NL and 2C cross zero at the same r-value, demonstrating that 2C predicts the instability threshold in NL. (b) QL growth rates as functions of r for $Pr = 1$ and four values of Γ. Growth rates in QL appear to increase without bound as r increases and cross zero for some r for each Γ. These properties are inconsistent with those of growth rates in NL and 2C, which are bounded from above as functions of r for sufficiently large Γ. (c) NL, 2C, and QL growth rates for $(Pr, r) = (1, 3)$ as functions of Γ. Growth rates in 2C show good agreement with those of NL and decrease with Γ. QL growth rates also decrease with Γ, but maintain much larger values than those in NL and 2C. This figure demonstrates that the EENL feedback substantially reduces instability growth rates and is necessary for the boundedness of growth rates from above as a function of r which results in elimination of the instability for all r beyond a threshold value of Γ.

evaluate the role of this EENL feedback in the elimination of the mean flow formation instability, we now construct a model bridging the QL and NL dynamics which we refer to as the 2-component model (2C). In this model, the NL system is used to obtain the symmetric convection equilibrium state. Once equilibrium has been attained, a mean flow perturbation is added and all horizontal components beyond the first two ($n \geq 3$) are "frozen," so that they do not vary for the remainder of the numerical experiment. Although this procedure is unphysical, it allows us to isolate the effects of the tilting and EENL feedbacks, which involve only the first two components, from all other aspects of the dynamics.

The mean flow energy growth rates in the 2C model (solid curves) and the NL system (discrete symbols) for $Pr = 1$ and varying (Γ, r) are shown in Fig. 5(a). For $\Gamma = 1.20$ and $\Gamma = 1.35$, growth rates in NL and 2C cross zero at the same r-values, demonstrating that, for low Γ, the 2C model captures the transition to the mean flow state that occurs in NL. As Γ is increased, growth rates in NL and 2C are displaced toward more negative values. The growth rate curves pass entirely below zero as Γ is increased beyond $\Gamma \approx 1.4$, providing an explanation for the observed disappearance of the mean flow bifurcation in NL seen by comparing Figs. 2(a) and 2(b). For $\Gamma = 1.35$ and $\Gamma = 1.50$, growth rates in NL exhibit maxima as functions of r, decreasing slowly as r is increased beyond the maximum. Growth rates in the 2C model are in close agreement with those of the NL system for low r and also attain a maximum prior to decreasing as r is increased, although this decrease of growth rate occurs more rapidly in 2C than in the NL system.

A necessary condition for the elimination of the tilting instability for all r is that the mean flow growth rate is bounded from above as a function of r. Figure 5(b) shows mean flow energy growth rates in the QL model. As in NL and 2C, instability growth rates in the QL model decrease with increasing Γ. However, growth rates in QL appear to increase without bound as r increases, and thus fail to reproduce the decreasing behavior found in NL and 2C for sufficiently large r and Γ. As a result, increasing Γ in the QL system displaces the transition to the mean flow state to higher values of r, rather than eliminating the instability completely as occurs in NL and 2C. This can also be seen by comparing the QL bifurcation diagrams in Figs. 2(a) and 2(b). For $\Gamma = 0.5$, the QL system transitions to the mean flow state near $r \approx 1.05$. For $\Gamma = 2$, the continued increase of growth rate

with r in QL leads to a mean flow bifurcation in QL, but with the bifurcation point displaced to $r \approx 2.7$. The agreement of the NL and 2C systems on the boundedness of growth rates and the absence of this property in QL provide evidence that the EENL suppression feedback is responsible for the elimination of the mean flow instability at large Γ.

Our understanding of the physical mechanisms controlling the mean flow growth rate and its dependence on Γ can be further improved by comparing growth rates in the NL, 2C, and QL systems as functions of Γ for fixed r, shown in Fig. 5(c) for $r = 3$. The 2C model quantitatively captures the decrease of growth rate with Γ observed in NL, demonstrating that the dynamics of the first two horizontal Fourier components are sufficient to capture the behavior of NL in the vicinity of the instability threshold over a moderate range of Γ. On the other hand, growth rates in the QL model maintain much larger values than those in NL and 2C, showing qualitative but not quantitative agreement with growth rates in the NL system. The quantitative difference between the growth rates in QL and those of NL and 2C demonstrates that the inclusion of the EENL feedback substantially reduces the strength of the mean flow instability. The decrease of growth rate with Γ in QL demonstrates that the tilting instability weakens with increasing Γ even in the absence of EENL effects. This weakening is due in large part to the suppression of roll tilting by the vertical advection feedback, which we discuss in Sec. V. This vertical advection mechanism is also present in the NL and 2C systems, and contributes together with the EENL feedback to reducing growth rates in NL and 2C for large Γ.

The difference in mean flow formation properties of the QL and NL systems seen in Figs. 1, 2, and 5 could be attributed to two conceptually different possibilities. In the first possibility, the equilibrium state of steady symmetric convection occurring in NL could differ from that of QL so that the NL state is stable while the QL state is unstable. In the second possibility, the equilibrium states could be similar in QL and NL, but the linear dynamics of the NL system could differ from those of QL so that the NL system is stable while the QL system is unstable. We argue here that it is the second possibility, the difference in linear dynamics between NL and QL, that is responsible for the difference in behavior in this problem. Although the symmetric equilibrium states of QL and NL differ somewhat due to the weak nonlinear excitation of higher wavenumber components in NL at low Ra, additional experiments (not shown) demonstrate that the linear QL dynamics continues to produce a mean flow even when the QL equilibrium state is replaced by the NL equilibrium state. This indicates that the small differences in equilibrium states between QL and NL are not responsible for their differences in mean flow formation.

We have argued that a particular interaction within the linear dynamics of NL, the EENL feedback, is responsible for the suppression of mean flows in NL for sufficiently large Γ. In the conceptual framework outlined above, this feedback is the specific instance of differing linear dynamics that explains the differences between the behavior of the NL and QL systems in 2D convection. The analysis in Sec. IV compares the results of the 2C model, which includes the EENL feedback but discards much of the rest of the linearized dynamics of NL, with those of the full NL system and the QL model. This comparison demonstrates that retaining only the subset of interactions contained in the 2C model is sufficient to quantitatively reproduce the mean flow suppression observed in the NL system. Further, the QL model does not show mean flow suppression, so that the mechanism responsible for mean flow suppression must be included in NL and 2C but not in QL. These results support our conclusion that the EENL feedback, which is included in NL and 2C but not in QL, is responsible for the suppression of mean flows in the NL system.

V. MECHANISM OF ELIMINATION OF THE MEAN FLOW INSTABILITY IN LOW-ORDER MODELS

Many LOMs of 2D convection exhibit elimination of the mean flow instability for all r for large Γ similar to that occurring in the NL system. This presents a puzzle, since we have demonstrated in Secs. III and IV that the EENL feedback is necessary for instability elimination in NL, but LOMs exhibit elimination while excluding this feedback. Further, LOMs can show instability elimination even though they are equivalent to Fourier truncations in the vertical of the QL model, which does not show instability elimination. In this section, we demonstrate that the physical mechanism responsible

for the elimination of the mean flow instability in LOMs is a negative feedback involving vertical advection. We show that this feedback is excessively strong in certain LOMs as a result of their low resolution, and that this excessive strength results in instability elimination. On the other hand, the QL model contains an adequately resolved vertical advection feedback and does not show instability elimination, consistent with the exclusion of the EENL feedback from the QL model. We clarify the role of the vertical advection feedback in the mean flow instability, and its dependence on model resolution, by examining growth rates, as well as relevant structures and tendencies, in the H95 LOM and the QL model for $(\Gamma, Pr) = (4, 1)$, representative parameter values for which a strong mean flow is formed in QL beyond $r \approx 8$ while mean flows are suppressed in NL and H95 for all r.

The H95 model includes the seven Fourier components $(A_{01,\,03,\,12},\ B_{11},\ C_{02,\,11},\ D_{12})$ in the notation of Sec. II C. This choice of truncation resulted from the addition of the A_{03} component to the HK86 LOM, which does not exhibit elimination of the mean flow instability. Inclusion of the A_{03} component permits the mean flow to take on a more realistic vertical structure, and was added to HK86 to enforce conservation of total vorticity.[21] Figure 6(a) (circles) shows the mean flow energy growth rate as a function of r in the H95 model, which we also refer to as $\mathrm{H95}_{12}$ when required

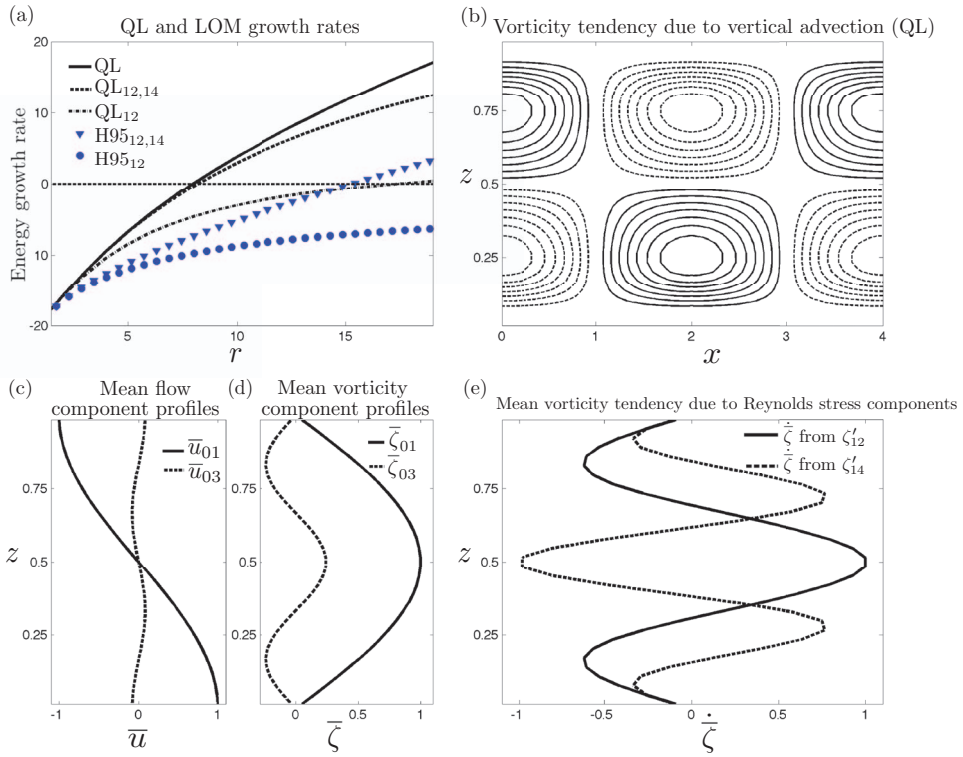

FIG. 6. Mean flow suppression behavior and mechanism operating in QL and LOMs. (a) Growth rates as functions of r for $(\Gamma, Pr) = (4, 1)$ in the QL model and its truncations QL_{12} and $\mathrm{QL}_{12,14}$ alongside those in the $\mathrm{H95}_{12}$ model and its extension $\mathrm{H95}_{12,14}$. These growth rate curves demonstrate that in both the QL and H95 model groups, growth rates are reduced as the number of Fourier components retained in the vertical is reduced. In particular, the low-resolution model $\mathrm{H95}_{12}$ exhibits complete instability suppression for these parameter values, while the higher-resolution model $\mathrm{H95}_{12,14}$ does not exhibit such an instability cutoff. (b) Normalized vorticity tendency due to vertical advection of the mean vorticity by the symmetric roll, sampled during mean flow growth for $(\Gamma, Pr, r) = (4, 1, 15)$ in QL. Solid contours indicate positive values. This tendency structure is close to the negative of the tilting vorticity and so suppresses the tilting of convection (cf. Fig. 4(c)). (c) Normalized profiles (relative scaling retained) of the first (solid) and second (dashed) vertical Fourier components of the mean flow part of the growing eigenstructure on the symmetric roll state. (d) Mean vorticity profiles associated with the structures shown in (c). (e) Mean vorticity tendencies arising from the first (solid) and second (dashed) components of the tilting vorticity. The first tendency component projects positively while the second tendency component projects negatively on the second mean vorticity component $\bar{\zeta}_{03}$. This figure demonstrates that the vertical advection feedback responsible for the instability cutoff in LOMs is excessively strong as a result of poor resolution, and that increasing resolution eliminates the instability cutoff in these LOMs.

for clarity. The growth rate remains negative over all r, coming to a horizontal asymptote near -2, demonstrating the elimination of the mean flow instability for $(\Gamma, Pr) = (4, 1)$ in the H95 model.

To understand the force that opposes the tilting of convection rolls in H95, it is useful to examine the QL eddy vorticity equation (13) linearized about the symmetric convection state. Denoting fixed point quantities with a star and linear perturbations with a δ we have

$$\frac{\partial}{\partial t}\nabla^2\delta\psi' = -\delta\overline{u}\frac{\partial}{\partial x}\nabla^2\psi'^{\star} + w'^{\star}\frac{\partial^2}{\partial z^2}\delta\overline{u} + RaPr\frac{\partial}{\partial x}\delta\theta' + Pr\nabla^4\delta\psi'. \tag{21}$$

The first term on the RHS is the advection of the eddy vorticity perturbation by the mean flow and acts to tilt the convection rolls, while the second term is the vertical advection of the mean vorticity perturbation by the background convection. This vertical advection interaction provides an important negative feedback on mean flow formation which ultimately results in the instability cutoff in H95. Figure 6(b) shows the structure of the vorticity tendency due to vertical advection during mean flow growth in QL for $r = 15$, normalized to unit amplitude. The tilting vorticity field is not shown, but closely resembles Fig. 4(c). The vorticity tendency due to vertical advection projects strongly negatively on the tilting vorticity, weakening the mean flow formation feedback.

The vertical structure of the mean flow is critical to the vertical advection effect. The first two vertical Fourier components of the growing mean flow in QL ($\overline{u}_{01}$ and $\overline{u}_{03}$) are shown in Fig. 6(c). The profiles are normalized with their relative scaling retained. Although the first component $\overline{u}_{01}(z) \propto \cos(\pi z)$ is visibly dominant over the second component $\overline{u}_{03} \propto \cos(3\pi z)$, the second component remains relevant to the vertical advection effect since its larger vertical wavenumber leads to an enhanced vorticity signature. Mean vorticity profiles for these two mean flow components ($\overline{\zeta}_{01}$ and $\overline{\zeta}_{03}$) are shown for QL in Fig. 6(d). Each component contributes to the eddy vorticity tendency through both the tilting and vertical advection parts of the advective interaction in (21). The first component $\overline{\zeta}_{01}$ has the net effect of supporting tilt formation for all Ra, Γ. The second component $\overline{\zeta}_{03}$ can either enhance or suppress the instability depending on Γ, with suppression occurring beyond $\Gamma \approx 1/\sqrt{2}$. As demonstrated by Hermiz *et al.*,[21] suppression of roll tilting due to the presence of the $\overline{\zeta}_{03}$ component is responsible for the instability cutoff in H95.

Each mean flow component is driven by a Reynolds stress that varies linearly with the strength of the tilting circulation. Although the tilting vorticity structure is dominated by its first vertical Fourier component (which resembles Fig. 4(c)), higher components of the tilting field also contribute to the Reynolds stresses. Figure 6(e) shows the normalized mean vorticity tendencies due to the first ($\zeta'_{12} \propto \cos(kx)\sin(2\pi z)$, solid curve) and second ($\zeta'_{14} \propto \cos(kx)\sin(4\pi z)$, dashed curve) tilting components, with their relative scaling retained. The mean vorticity tendency due to the first tilting component ζ'_{12} projects positively onto the second mean vorticity component $\overline{\zeta}_{03}$. Since $\overline{\zeta}_{03}$ suppresses tilting through the vertical advection effect, this constitutes a negative feedback that suppresses tilting of the rolls. However, the mean vorticity tendency due to the second tilting component ζ'_{14} projects negatively onto $\overline{\zeta}_{03}$, weakening this negative feedback. If the ζ'_{14} component of the tilting vorticity is not retained in a LOM, the negative feedback due to vertical advection will be excessively strong due to the absence of the weakening effect arising from ζ'_{14}. This unrealistically strong feedback provides the physical mechanism by which the inclusion of the higher mean flow component $\overline{\zeta}_{03}$ in LOMs produces an instability cutoff.

We have shown above that vertical advection of the mean flow by the rolls produces a negative feedback on mean flow formation and that the Reynolds stress arising from the second vertical component of the tilting vorticity acts to weaken this negative feedback. We now demonstrate that this weakening effect strongly influences mean flow instability growth rates, and that the absence of the weakening effect in LOMs can result in elimination of the mean flow instability for all r for sufficiently large Γ. The H95 LOM does not include the second vertical component of the tilting vorticity, and so excludes the weakening effect on the vertical advection feedback due to this component. The impact of augmenting the H95 model to include the second tilting component (A_{14}, D_{14}) can be seen in Fig. 6(a) (triangles), which shows the growth rate for this augmented model. For clarity, we refer to this augmented model as $\mathrm{H95}_{12,14}$ and to the original H95 model as $\mathrm{H95}_{12}$. Based on the discussion above, it is expected that this increase in resolution will weaken the suppressing vertical advection feedback and increase the instability growth rate in $\mathrm{H95}_{12,14}$ relative

to that of $H95_{12}$. $H95_{12,14}$ growth rates are indeed enhanced relative to those of $H95_{12}$ and cross zero near $r = 15$, the instability cutoff having been eliminated in agreement with the absence of a cutoff in the QL model. This provides evidence that the strength of the vertical advection feedback strongly influences the tilting instability in LOMs. However, growth rates in $H95_{12,14}$ still differ substantially from those of the full QL model (Fig. 6(a), solid). To test that growth rates in QL are controlled by the same mechanisms as those operating in LOMs, a numerical experiment was conducted (QL_{12}) in which the tilting vorticity field was projected onto its first Fourier component (ζ'_{12}) before computing its associated Reynolds stress. This procedure filters contributions to the Reynolds stress from higher components of the tilting field, similar to retaining only the first tilting Fourier component in a LOM. Based on the observation in LOMs that reduced resolution of the tilted convection results in an artificially strengthened vertical advection feedback, it is expected that the instability growth rates will be weakened in QL_{12} relative to those of QL. The QL_{12} growth rate curve is shown in Fig. 6(a) (dotted-dashed). Although the instability is not prevented entirely in QL_{12}, the growth rates are strongly suppressed relative to those of the full QL model. In contrast, a further experiment in which Reynolds stress contributions from both the first and second vertical Fourier components of the tilting vorticity (ζ'_{12} and ζ'_{14}) were retained ($QL_{12,14}$, Fig. 6(a), dashed) showed quantitative agreement with QL growth rates over a large range of r and accurately predicted the location of the bifurcation point itself. These experiments with QL, QL_{12}, and $QL_{12,14}$ indicate that instability growth rates in the quasilinear dynamics are largely determined by an interplay between the positive effect of the tilting feedback, the negative effect of the vertical advection feedback, and the weakening of the vertical advection feedback by the second vertical Fourier component of tilted convection. Based on the above discussion, we conclude that the observed qualitative differences between commonly used LOMs such as H95 and the full QL model can be attributed to the excessive strength of the vertical advection feedback in LOMs resulting from poorly resolved convection.

VI. SUMMARY AND DISCUSSION

It is well known that the 2D laminar convection rolls occurring in 2D Rayleigh-Bénard convection and related systems can form mean flows by the tilting mechanism. Mean flows of this type have been found to form in periodic domains only when the aspect ratio Gamma is sufficiently low, but no mechanistic explanation for this Γ-dependence has previously been given. In addition, the Γ-dependence of the mean flow instability is reproduced by some simplified theoretical models but not others: while the simplest LOMs and the QL model form mean flows for all Γ, more complex LOMs typically exhibit elimination of the mean flow instability for large Γ. As LOMs commonly serve as conceptual tools for understanding this system, it is important to clarify the relationship between the physical mechanisms operating in LOMs, QL, and NL. In this work, we have addressed these issues by using numerical results from the NL system, the QL model, and selected LOMs to identify the physical mechanisms central to the mean flow instability in each system and to assess their effects on the instability growth rate.

We found that the elimination of the mean flow instability for large Γ in NL, and the absence of this elimination in QL, results from EENL interactions that are included in NL but not in QL. For low Γ, transition to the mean flow state occurs in NL for marginally supercritical values of *Ra*. This behavior is mirrored in QL which agrees quantitatively with NL on both the instability growth rate and equilibrated amplitude, consistent with the theoretical predictions of Rosenbluth and Shapiro.[28] When Γ is sufficiently increased, mean flow formation ceases to occur in NL, instead being replaced by the presence of symmetric convection rolls stable to much higher *Ra*. On the other hand, strong mean flows continue to form in QL for large Γ, indicating that the mean flow suppression mechanism is absent from the QL model. In the QL dynamics, the nonlinear interaction between the mean flow and the convection is retained, but EENL interactions are neglected. We therefore conclude that the suppression mechanism arises from the EENL interactions that are filtered in QL. The particular stabilizing feedback is due to the EENL interaction of the symmetric rolls (dominated by the $n = 1$ horizontal Fourier component) with the $n = 2$ horizontal Fourier component of the flow. The role of this EENL feedback in the dynamics of mean flow formation may be understood by considering the following numerical experiment: To the equilibrated roll state, a mean flow perturbation is added

with amplitude $\mathcal{O}(\varepsilon)$. Advection of the $n = 1$ rolls by the mean flow produces an $n = 1$ perturbation vorticity field at $\mathcal{O}(\varepsilon)$ associated with roll tilting. This tilting perturbation yields an $\mathcal{O}(\varepsilon)$ Reynolds stress reinforcing the shear. This forcing of the mean flow is referred to as the tilting mechanism. At the same time, a negative feedback operates through a pathway involving two EENL interactions. In the first of these, the EENL interaction of the $n = 1$ symmetric rolls with the $n = 1$ tilting perturbation generates an $n = 2$ vorticity field at $\mathcal{O}(\varepsilon)$. In the second, the EENL interaction of this $n = 2$ structure with the $n = 1$ symmetric rolls projects negatively onto the tilting perturbation at $\mathcal{O}(\varepsilon)$. This EENL vorticity tendency suppresses the tilting of the rolls and provides a negative feedback preventing mean flow formation as Γ increases sufficiently.

To demonstrate that the EENL feedback mechanism is responsible for the cutoff of the mean flow instability for large Γ in NL, we constructed the simplified 2C model. In this model, the symmetric convection equilibrium state was obtained using the NL dynamics, and the linear dynamics of the mean flow and the $n = 1$ and $n = 2$ horizontal Fourier components of convection were analyzed upon this background. The 2C model was found to accurately reproduce the growth rates of NL over a range of *Ra*-values in the vicinity of the instability threshold. Furthermore, growth rates in the 2C model are bounded from above as functions of *Ra*, again reproducing the behavior of growth rates in NL. On the other hand, growth rates in the QL model appear to increase without bound as *Ra* is increased. Boundedness of growth rates from above is necessary for elimination of the mean flow instability for all *Ra* for sufficiently large Γ. The absence of such boundedness from the QL model, together with its presence in the 2C system, provides evidence that the EENL negative feedback mechanism is responsible for instability elimination in the NL and 2C systems. Although growth rates in the QL model are unbounded as *Ra* increases, the QL model qualitatively reproduces the decrease of growth rate with Γ seen in NL and 2C. Together, the results of the NL, 2C, and QL models indicate that the most important physical effects determining mean flow growth rates are the tilting and vertical advection feedbacks, which involve the $n = 1$ component only, as well as the negative feedback arising from the coupling between the $n = 1$ and $n = 2$ components, which is responsible for elimination of the mean flow instability for all *Ra* for sufficiently large Γ.

Berning and Spatschek[33] previously noted that the $(n, m) = (2, 1)$ Fourier component could prevent mean flow formation when added to LOMs. They also found that this mean flow suppression effect was unique to the (2, 1) component: no other component, when added to LOMs, produced similar mean flow suppression. The (2, 1) component is the central component involved in the EENL suppression feedback discussed in this paper, and has a similar structure to that shown in Fig. 4(d). The analysis of Berning and Spatschek[33] thus supports the conclusion of this work that the EENL feedback is responsible for the elimination of the tilting instability in the NL system. However, they attributed the suppression effect of the (2, 1) component to the fact that this component becomes linearly unstable as an eigenmode on the conduction state before the tilting component as *Ra* is increased. However, since mean flows form as a secondary instability on the equilibrated roll state, the growth rate of a structure on the conduction state is not obviously linked to its role in the suppression mechanism.

In Sec. V, we turned to a discussion of the physical mechanisms important to mean flow formation in LOMs. We found that although complete mean flow suppression for large Γ occurs in many LOMs, the physical mechanism of suppression must differ from that of NL as LOMs typically do not retain horizontal Fourier components beyond $n = 1$, thereby excluding the EENL feedback. As previously noted by Takagi and Matsuda,[34] vertical advection of the mean flow profile by the symmetric rolls inhibits roll tilting, providing a negative feedback on mean flow formation. We showed that although this feedback can prevent mean flow formation in LOMs, the complete instability suppression for large Γ observed in some LOMs is due to excessively strong vertical advection feedbacks in those models. Although the QL dynamics also contains the vertical advection feedback, it does not exhibit elimination of the mean flow instability. This difference arises because in QL, the mean flow component most important to the vertical advection feedback is weakened by the Reynolds stress arising from the second vertical Fourier component of the tilting perturbation, a feature of convection that is unresolved in most LOMs. As a result, the positive effect of the tilting feedback outcompetes the negative effect of vertical advection in QL so that mean flows form for all values of Γ for sufficiently large r. While LOMs remain useful tools for understanding 2D

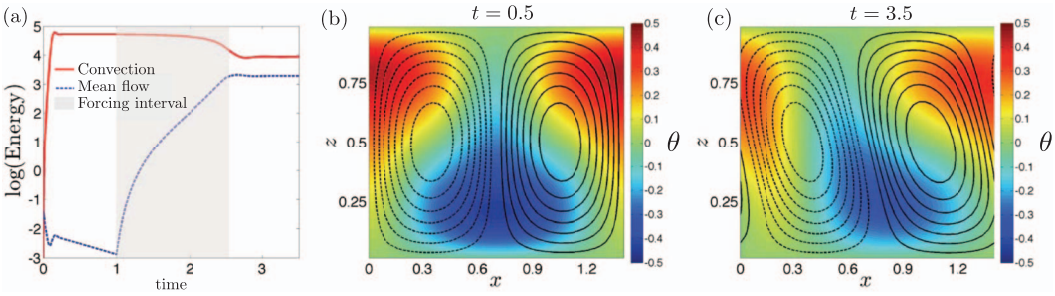

FIG. 7. Example of multiple equilibria in the NL system for (Γ, Pr, r) = (1.4, 1, 3). (a) Time series of convection and mean flow energies during a forcing experiment in which a body force is applied to drive the mean flow during the interval $t \in [1, 2.5]$ (shaded). Prior to the application of the body force, the mean flow decays exponentially indicating stability of the convective state. After the body force is removed, the mean flow remains stable at finite amplitude. (b) Symmetric convection equilibrium state sampled at $t = 0.5$. Solid contours show eddy streamlines with counter-clockwise circulation, shading shows the buoyancy field. (c) Tilted convection equilibrium state with mean flow sampled at $t = 3.5$. This figure demonstrates that tilted convection equilibria with mean flows may be stable for parameter values for which symmetric convection equilibrium states are also stable.

convection, care must be exercised in their use, as they may reproduce phenomena observed in NL via fundamentally different underlying mechanisms.

In this work, we have studied convection-driven mean flows with a focus on the tilting instability of steady symmetric convection. However, stable mean flow states can, in fact, exist in the NL system even in parameter regimes for which the growth rate of mean flow perturbations upon the symmetric equilibrium state is negative for all r. Although the EENL feedback prevents the growth of infinitesimal perturbations for sufficiently large Γ, a finite-amplitude perturbation can send the system into an alternate mean flow equilibrium. Figure 7 shows an example of multiple equilibrium behavior for (Γ, Pr, r) = (1.4, 1, 3). After the initial convective instability, the mean flow decays exponentially, indicating that the symmetric convection equilibrium state shown in Fig. 7(b) is stable. For $t \in [1, 2.5]$ (shaded), a body force proportional to $\cos(\pi z)$ is applied to the mean flow. Beyond $t = 2.5$ the system freely evolves under the NL dynamics and remains in the stable tilted convection equilibrium state with mean flow shown in Fig. 7(c). We did not attempt to comprehensively map the parameter subspace in which multiple equilibria exist, but stable mean flow states became more difficult to locate as Γ was increased, which we take as an indication that the parameter subspace exhibiting such equilibria contracts in size with increasing Γ. We were unable to obtain multiple equilibria below $r = 10$ for $\Gamma > 1.7$ and $Pr = 1$.

The existence of multiple equilibria is a common phenomenon in nonlinear systems, and has been previously found to occur in Rayleigh-Bénard convection in connection with mean flows. Knobloch and Guckenheimer[35] and Busse and Or[36] discovered a family of solutions associated with resonant interactions at relatively low Ra that are distinct from steady roll solutions. Resonant interactions, which occur when the aspect ratio is such that the conduction state becomes simultaneously unstable to two convective eigenmodes of different wavenumbers as Ra is increased, can produce mixed solutions which can be accompanied by mean flows. The role of these resonant interactions in producing a multiplicity of equilibrium states in Rayleigh-Bénard convection was thoroughly investigated using numerical continuation by Prat *et al.*,[37] who also identified the mean flow solutions. Mean flows produced through resonance, a mechanism distinct from the tilting mechanism occurring at low aspect ratio, play an important role in the wavenumber selection process, although such mean flow states have typically been found to be unstable.

The physical mechanisms discussed in this paper may have applications beyond the transition to a steady mean flow in the 2D Rayleigh-Bénard system. For example, thin film annular electroconvection provides an experimentally realizable 2D periodic convection system.[38] Results from recent simulations[39] have shown that 2D annular electroconvection yields roll circulations similar to those arising from thermal convection, but mean flow formation has not yet been found to occur in this system. The tilting, vertical advection, and EENL feedback mechanisms discussed here

are likely to play important roles in 2D electroconvection, as these mechanisms are generic to 2D roll circulations. The EENL feedback in particular may be responsible for mean flow inhibition in this system. The EENL feedback may also play a role in modifying the subsequent transitions to oscillatory tilted convection and relaxation oscillations[2] which occur in the 2D convection system. As these states arise from bifurcations of the steady mean flow state, the EENL feedback prevents their occurrence for large Γ, but may also influence the properties of these transitions in parameter regimes for which mean flow formation is not prevented entirely.

ACKNOWLEDGMENTS

The authors acknowledge support from the Natural Sciences and Engineering Research Council (J.F.) and the U.S. National Science Foundation (NSF) (B.F.) under Grant Nos. NSF AGS-1246929 and ATM-0736022. The authors also thank two anonymous reviewers for helpful comments.

[1] R. Thompson, "Venus's general circulation is a merry-go-round" J. Atmos. Sci. **27**, 1107–1116 (1970).
[2] J. M. Finn, "Nonlinear interaction of Rayleigh–Taylor and shear instabilities," Phys. Fluids B **5**, 415–432 (1993).
[3] J. Prat, J. M. Massaguer, and I. Mercader, "Large-scale flows and resonances in 2-D thermal convection," Phys. Fluids **7**, 121–134 (1995).
[4] N. Bian, S. Benkadda, O. E. Garcia, J.-V. Paulsen, and X. Garbet, "The quasilinear behavior of convective turbulence with sheared flows," Phys. Plasmas **10**, 1382–1388 (2003).
[5] N. E. Hurlburt, J. Toomre, and J. M. Massaguer, "Two-dimensional compressible convection extending over multiple scale heights," Astrophys. J. **282**, 557–573 (1984).
[6] G. P. Ginet and R. N. Sudan, "Numerical observations of dynamic behaviour in two-dimensional compressible convection," Phys. Fluids **30**, 1667–1677 (1987).
[7] M. R. E. Proctor, N. O. Weiss, D. P. Brownjohn, and N. E. Hurlburt, "Nonlinear compressible magnetoconvection Part 2. Streaming instabilities in two dimensions," J. Fluid Mech. **280**, 227–253 (1994).
[8] S. R. Lantz and R. N. Sudan, "Magnetoconvection dynamics in a stratified layer. I: Two-dimensional simulations and visualization," Astrophys. J. **441**, 903–924 (1995).
[9] A. Rucklidge, M. Proctor, and J. Prat, "Mean flow instabilities of two-dimensional convection in strong magnetic fields," Geophys. Astrophys. Fluid Dyn. **100**, 121–137 (2006).
[10] W. Horton, G. Hu, and G. Laval, "Turbulent transport in mixed states of convective cells and sheared flows," Phys. Plasmas **3**, 2912–2923 (1996).
[11] J. M. Finn, J. F. Drake, and P. N. Guzdar, "Instability of fluid vortices and generation of sheared flow," Phys. Fluids B **4**, 2758–2768 (1992).
[12] L. N. Howard and R. Krishnamurti, "Large-scale flow in turbulent convection: A mathematical model," J. Fluid Mech. **170**, 385–410 (1986).
[13] P. Tabeling, O. Cardoso, and B. Perrin, "Chaos in a linear array of vortices," J. Fluid Mech. **213**, 511–530 (1990).
[14] T. Hartlep, A. Tilgner, and F. H. Busse, "Transition to turbulent convection in a fluid layer heated from below at moderate aspect ratio," J. Fluid Mech. **544**, 309–322 (2005).
[15] N. H. Bian and O. E. Garcia, "Confinement and dynamical regulation in two-dimensional convective turbulence," Phys. Plasmas **10**, 4696–4707 (2003).
[16] J. Werne, "Structure of hard-turbulent convection in two dimensions: Numerical evidence," Phys. Rev. E **48**, 1020–1035 (1993).
[17] In the case of convection driven by periodic internal heating[4] or by periodic internal mechanical forcing,[13] the spatial scale of convection is determined by the forcing scale rather than by Γ. However, given this scale, a similar dependence of mean flow formation on the convection scale would be expected.
[18] F. H. Busse, "On the mean flow induced by a thermal wave," J. Atmos. Sci. **29**, 1423–1429 (1972).
[19] E. N. Lorenz, "Deterministic nonperiodic flow," J. Atmos. Sci. **20**, 130–141 (1963).
[20] R. Krishnamurti and L. N. Howard, "Large-scale flow generation in turbulent convection," Proc. Natl. Acad. Sci. U.S.A. **78**, 1981–1985 (1981).
[21] K. B. Hermiz, P. N. Guzdar, and J. M. Finn, "Improved low-order model for shear flow driven by Rayleigh-Bénard convection," Phys. Rev. E **51**, 325–331 (1995).
[22] J.-L. Thiffeault and W. Horton, "Energy-conserving truncations for convection with shear flow," Phys. Fluids **8**, 1715–1719 (1996).
[23] A. Gluhovsky, C. Tong, and E. Agee, "Selection of modes in convective low-order models," J. Atmos. Sci. **59**, 1383–1393 (2002).
[24] A. Gluhovsky and C. Tong, "The structure of energy conserving low-order models," Phys. Fluids **11**, 334–343 (1999).
[25] J. F. Drake, J. M. Finn, P. Guzdar, V. Shapiro, V. Shevchenko, F. Waelbroeck, A. B. Hassam, C. S. Liu, and R. Sagdeev, "Peeling of convection cells and the generation of sheared flow," Phys. Fluids B **4**, 488–491 (1992).
[26] S. R. Lantz, "Magnetoconvection dynamics in a stratified layer. II: A low-order model of the tilting instability," Astrophys. J. **441**, 925–941 (1995).
[27] A. M. Rucklidge and P. C. Matthews, "Analysis of the shearing instability in nonlinear convection and magnetoconvection," Nonlinearity **9**, 311 (1996).
[28] M. N. Rosenbluth and V. D. Shapiro, "Analytical model of the "tilting" instability," Phys. Plasmas **1**, 222–224 (1994).

[29] G. I. Soloviev, V. D. Shapiro, R. C. J. Somerville, and B. Shkoller, "The tilting instability with buoyant forcing in a two-dimensional viscous fluid," J. Atmos. Sci. **53**, 2671–2684 (1996).
[30] K. Srinivasan and W. R. Young, "Zonostrophic instability," J. Atmos. Sci. **69**, 1633–1656 (2012).
[31] J. R. Herring, "Investigation of problems in thermal convection," J. Atmos. Sci. **20**, 325–338 (1963).
[32] Time-dependent horizontal mean flows without this antisymmetry have also been found to form in Rayleigh-Bénard convection.[3,40] These mean flows without antisymmetry can develop at higher Γ and form through a bifurcation taking place at much higher r. This bifurcation occurs from a state of time-dependent convection without a mean flow component to a chaotic or quasiperiodic state including a mean flow component. As we are interested in mean flow formation by the tilting instability at low r, we focus here on the antisymmetric case.
[33] M. Berning and K. H. Spatschek, "Bifurcations and transport barriers in the resistive-g paradigm," Phys. Rev. E **62**, 1162–1174 (2000).
[34] M. Takagi and Y. Matsuda, "Interpretation of Thompson's mechanism for Venus' atmospheric super-rotation and its extension to the spherical geometry," J. Meteor. Soc. Jpn. **77**, 971–983 (1999).
[35] E. Knobloch and J. Guckenheimer, "Convective transitions induced by a varying aspect ratio," Phys. Rev. A **27**, 408–417 (1983).
[36] F. H. Busse and A. C. Or, "Subharmonic and asymmetric convection rolls," Z. Angew. Math. Phys. **37**, 608–623 (1986).
[37] J. Prat, I. Mercader, and E. Knobloch, "Resonant mode interactions in Rayleigh-Béenard convection," Phys. Rev. E **58**, 3145–3156 (1998).
[38] Z. A. Daya, V. B. Deyirmenjian, S. W. Morris, and J. R. de Bruyn, "Annular electroconvection with shear," Phys. Rev. Lett. **80**, 964–967 (1998).
[39] P. Tsai, Z. A. Daya, V. B. Deyirmenjian, and S. W. Morris, "Direct numerical simulation of supercritical annular electroconvection," Phys. Rev. E **76**, 026305 (2007).
[40] E. Zienicke, N. Seehafer, and F. Feudel, "Bifurcations in two-dimensional Rayleigh-Bénard convection," Phys. Rev. E **57**, 428–435 (1998).